

Evidence for charge delocalization crossover in the quantum critical superconductor CeRhIn₅

Honghong Wang^{1,2#}, Tae Beom Park^{1,2,3#}, Jihyun Kim^{1,2}, Harim Jang^{1,2},
Eric D. Bauer⁴, Joe D. Thompson^{4†}, Tuson Park^{1,2†}

¹*Center for Quantum Materials and Superconductivity (CQMS), Sungkyunkwan University, Suwon 16419, South Korea*

²*Department of Physics, Sungkyunkwan University, Suwon 16419, South Korea*

³*Institute of Basic Science, Sungkyunkwan University, Suwon 16419, South Korea*

⁴*Los Alamos National Laboratory, Los Alamos, NM 87545, USA*

[#]*These authors contributed equally: Honghong Wang, Tae Beom Park*

[†]*email: jdt@lanl.gov; tp8701@skku.edu*

The nature of charge degrees-of-freedom distinguishes scenarios for interpreting the character of a second order magnetic transition at zero temperature, that is, a magnetic quantum critical point (QCP). Heavy-fermion systems are prototypes of this paradigm, and in those, the relevant question is where, relative to a magnetic QCP, does the Kondo effect delocalize their f -electron degrees-of-freedom. Herein, we use pressure-dependent Hall measurements to identify a finite-temperature scale E_{loc} that signals a crossover from f -localized to f -delocalized character. As a function of pressure, $E_{\text{loc}}(P)$ extrapolates smoothly to zero temperature at the antiferromagnetic QCP of CeRhIn₅ where its Fermi surface reconstructs, hallmarks of Kondo-breakdown criticality that generates critical magnetic and charge fluctuations. In 4.4% Sn-doped CeRhIn₅, however, $E_{\text{loc}}(P)$ extrapolates into its magnetically ordered phase and is decoupled from the pressure-induced magnetic QCP, which implies a spin-density-wave (SDW) type of criticality that produces only critical fluctuations of the SDW order parameter. Our results demonstrate the importance of experimentally determining E_{loc} to characterize quantum criticality and the associated consequences for understanding the pairing mechanism of superconductivity that reaches a maximum T_c in both materials at their respective magnetic QCP.

The Kondo singlet is a quantum state in which spins of surrounding conduction electrons collectively screen a local moment through their antiferromagnetic (AFM) exchange. Theoretically expected and experimentally confirmed^{1,2}, the cloud of screening conduction electrons around a Kondo impurity extends radially to a distance $\xi = \hbar v_F / k_B T_K$, where v_F is the conduction electron Fermi velocity and $k_B T_K$ is the energy scale of singlet formation. ξ can be up to micrometers and certainly greater than interatomic spacing. In the many-body process of Kondo-singlet formation, the spin of the local moment becomes part of the conduction electron Fermi volume. For a periodic lattice of Kondo impurities, typified by f -electron heavy-fermion metals, quantum coherence among Kondo singlets (qualitatively, a Bloch state of Kondo-screening clouds) results in the formation of highly entangled composite heavy quasiparticles as $T \rightarrow 0$ K and an increase in the Fermi volume that counts both the local moments and conduction electrons. Interactions within the narrow (of order meV) quasiparticle bands can lead to an instability, often a spin-density-wave (SDW), of the large Fermi volume. Tuning the SDW transition to $T = 0$ K by a non-thermal control parameter, such as pressure, magnetic field, or chemical substitution, allows access to a quantum critical point (QCP) in which quantum fluctuations of the SDW order parameter control physical properties to temperatures well above $T = 0$ K³⁻⁵. The transition from a SDW order to a paramagnetic state at $T = 0$ K has no effect on the Fermi volume. This picture of a SDW QCP ignores the role of a long-range Rudermann-Kittel-Kasuya-Yosida (RKKY) interaction I among local moments that is mediated by the same conduction electrons that produce a Kondo singlet. The RKKY interaction induces dynamical correlations among the local moments, inhibiting Kondo singlet formation and thus preventing the emergence of a large Fermi volume. The competition between Kondo and RKKY interactions can be characterized by a non-thermal tuning parameter $\delta = k_B T_K / I$ ^{6,7}. Relative to the Kondo scale, I , though always finite, is relatively insensitive to pressure, field, etc. so that the T - δ phase diagram illustrated in Fig. 1 for heavy-fermion systems is controlled primarily by changes in T_K .

The nature of quantum critical fluctuations at δ_c where the magnetic boundary $T_N(\delta)$ reaches $T = 0$ K changes qualitatively depending on the location of a crossover scale $E_{loc}(\delta)$ that separates an electronic state in which static Kondo entanglement breaks down because of RKKY interactions and the Fermi surface is small (FS_S) and a state with fully intact composite quasiparticles that produce a large Fermi surface (FS_L). Depending on the position of $E_{loc}(\delta)$,

the nature of the magnetic QCP at δ_c is either of the SDW or Kondo-breakdown type. In the SDW scenario (Fig. 1a), E_{loc} remains finite at the QCP and terminates inside the ordered phase; only magnetic degrees-of-freedom are quantum critical at δ_c^3 . In a Kondo-breakdown scenario (Fig. 1b), however, E_{loc} reaches zero temperature at the magnetic QCP and the concomitant reconstruction of the FS from small-to-large coincides with the onset of magnetic order, thus incorporating both charge and magnetic quantum fluctuations at the Kondo-breakdown QCP⁸⁻¹¹. The distinct difference between SDW and Kondo-breakdown criticality has fundamental consequences for interpreting the origin of new phases of matter that frequently emerge around a QCP as the system relieves the buildup of entropy.

Evidence for a Kondo-breakdown type of quantum criticality has been found in a few heavy-fermion materials, notably $\text{CeCu}_{6-x}\text{Au}_x$ ¹², YbRh_2Si_2 ^{13,14}, and CeRhIn_5 ^{15,16}; whereas, a phase diagram like that in Fig. 1a appears in CeIn_3 ¹⁷, Co-doped YbRh_2Si_2 ¹⁸ and Ir-doped CeRhIn_5 ^{19,20}. Among examples representative of Fig. 1b physics, a FS change at their QCP has been inferred from Hall measurements. In CeRhIn_5 , on the other hand, evidence for an abrupt change in FS as $T \rightarrow 0$ K has come from a pressure-dependent quantum oscillation study that directly probes the FS of CeRhIn_5 in which an abrupt reconstruction of the FS coincides with an AFM QCP^{15,21,22}. Evidence for the crossover scale $E_{\text{loc}}(\delta)$, characteristic of Kondo breakdown, has yet to be reported in CeRhIn_5 , opening the possibility that FS reconstruction could be a consequence of a change in FS topology resulting from the loss of magnetic order²³. Here, we probe the change in Hall effect via systematic control of external pressure to identify $E_{\text{loc}}(\delta)$ in CeRhIn_5 , thereby demonstrating clearly that its criticality is of the Kondo-breakdown type. Replacing 4.4% of the In atoms by Sn shifts $E_{\text{loc}}(\delta)$ such that it intersects the $T_N(P)$ boundary at finite temperature (Fig. 1a) and the magnetic criticality changes to the SDW type. Not only imposing a far more unambiguous interpretation of criticality in CeRhIn_5 , these discoveries point to a change in the nature of fluctuations leading to Cooper pairing in pure and Sn-doped CeRhIn_5 and to the importance of E_{loc} for confirming a theoretically proposed beyond-Landau framework to understand quantum criticality^{4,6}.

Results

Observation of E_{loc} in CeRhIn_5 . Previous Hall measurements of CeRhIn_5 were limited to 2.6 GPa close to the critical pressure, $P_c = 2.3$ GPa, at which the AFM transition T_N extrapolates

to $T = 0$ K and the superconducting transition temperature T_c reaches a maximum^{21,22,24}. Our measurements of the Hall coefficient R_H at $P < P_c$, Fig. 2a, are consistent with the primary features reported earlier²⁴. A local minimum in R_H at T^* (as indicated by purple arrows) signals the onset of short-range AFM spin correlations above T_N ^{25,26} and is suppressed together with T_N under pressure. Figure 2b shows R_H in the high-pressure regime ($P > P_c$) where a previously unidentified local minimum in R_H appears at T_L (as marked by the orange arrows) and moves to higher temperature as the system is tuned away from magnetic order with increasing pressure. (T_L appears well above the temperature below which the resistivity assumes a Fermi-liquid T^2 dependence¹⁶.) The Hall coefficient in a multiband system with magnetic ions, particularly a compensated heavy-fermion metal like CeRhIn₅, is not straightforward to interpret^{15,24,27}. Prior experiments rule out any significant asymmetric (skew) scattering in CeRhIn₅ at low temperatures and pressures below P_c ^{24,27}, leaving temperature- and pressure-dependent changes in the ordinary Hall contribution as the most likely origin of T_L . In a system like CeRhIn₅, the magnitude of the ordinary term can be influenced not only by changes in carrier density but also by scattering rates on different parts of the Fermi surface, details of the surface topology, and the presence of spin fluctuations. Likely, all contribute to some extent to the unusual temperature- and pressure-dependence of an ordinary Hall contribution at $P > P_c$ and to a change in the character of charge carriers at T_L .

A color-contour map of the absolute value of R_H ($|R_H|$) for CeRhIn₅ is displayed in the temperature–pressure (T – P) plane in Fig. 2c. In the low-pressure AFM regime, T^* and T_N smoothly extrapolate to $T = 0$ K at P_c , at which T_c and $|R_H|$ are a maximum. The existence of an AFM QCP at P_c , hidden by the pressure-induced superconducting dome, has been revealed explicitly by applying a magnetic field sufficient to suppress superconductivity^{21,22}. As shown in the figure, $T_L(P)$ extrapolates smoothly on the paramagnetic side of the diagram to $T = 0$ K at the magnetic QCP where, in the limit $T \rightarrow 0$ K, the FS reconstructs, de Haas-van Alphen (dHvA) frequencies increase, and the quasiparticle effective mass diverges¹⁵. These are all essential characteristics of a Kondo-breakdown QCP. The phase diagram in Fig. 2c coincides with the theoretically predicted phase diagram (Fig. 1b) if we identify $T_L(P)$ as $E_{loc}(P)$, i.e., a change in the nature of charge carriers at T_L is accompanied by a crossover from small-to-large Fermi surface with increasing pressure at finite temperature. Theoretically, E_{loc} appears at some temperature below the onset of heavy quasiparticle formation⁶, typically taken experimentally

to be signaled by the temperature T_{\max} where the magnetic resistivity reaches a maximum. In CeRhIn₅, $T_{\max}(P)$ is roughly 6.5 times $T_L(P)$ at $P > P_c$ ²⁸. Multiple experiments, including dHvA measurements¹⁵, suggest that CeRhIn₅ at $P = P_c$ is equivalent to the isostructural heavy-fermion superconductor CeCoIn₅ at $P = 0$ GPa²⁹. Recent Hall measurements argue that CeCoIn₅ at $P = 0$ GPa is very close to a QCP characterized by a localization/delocalization of $4f$ -electrons at a transition connecting two Fermi surfaces of different volumes³⁰. A minimum in its Hall coefficient evolves with pressure increasing from $P = 0$ GPa in very much the same way as $T_L(P)$ shown in Fig. 2b for CeRhIn₅ at $P > P_c$ ²⁴. Further, the pressure-dependent temperature of a Hall minimum tracks the delocalization crossover temperature determined by nuclear quadrupole resonance measurements in CeIn₃^{17,31}, providing additional support for associating the Hall minimum in CeRhIn₅ and CeCoIn₅ with a delocalization crossover at finite temperature. Finally, similar to T^* ²⁷, the influence of magnetic field on T_L (Supplementary Fig. 1) is negligible even though $|R_H|$ is suppressed, an observation arguing against a substantial contribution of magnetic fluctuations to determining T_L . Each of these further compels the identification of T_L with E_{loc} .

Quantum criticality in Sn-doped CeRhIn₅. We turn to the case of CeRhIn₅ with a Sn concentration of 0.044, CeRh(In_{0.956}Sn_{0.044})₅, labelled as Sn-doped CeRhIn₅ in the following. Figures 3a,b show the temperature dependence of the Hall coefficient R_H for Sn-doped CeRhIn₅ at representative pressures up to 2.25 GPa. R_H was obtained by applying a magnetic field of 5 T that completely suppresses superconductivity over the whole pressure range studied. Similar to pure CeRhIn₅, two characteristic temperatures T^* and T_L are revealed by a local minimum in R_H . In the low-pressure regime, T^* decreases monotonically with increasing pressure and becomes unresolvable at 1.0 GPa (Fig. 3a). At pressures higher than 1.0 GPa, another local minimum in R_H appears at T_L and increases with increasing pressure (Fig. 3b). We note that the field effects on T^* and T_L in Sn-doped CeRhIn₅ are negligible (Supplementary Fig. 3). A color-contour map of the amplitude of R_H ($|R_H|$) for Sn-doped CeRhIn₅ at 5 T is shown in the T - P plane in Fig. 3c, which is overlaid with the phase boundaries. The slight Sn doping leads to a decrease of T_N from 3.8 K for pure CeRhIn₅ to 2.1 K in the Sn-doped case at ambient pressure³². With applying pressure, T_N decreases gradually and extrapolates to a terminal critical pressure P_{c2} (~ 1.3 GPa) where pressure-induced superconductivity reaches a maximum T_c . Accompanying the suppression of T_N , $T^*(P)$ decreases with pressure and also extrapolates

to $T = 0$ K at P_{c2} , a response qualitatively similar to pure CeRhIn₅ in which $T^*(P)$ is associated with the development of short-range AFM correlations. With $T_L(P) \ll T_{\max}(P)$ (Supplementary Fig. 5 and $\partial T_L/\partial P > 0$ at $P \geq 1.2$ GPa (Fig. 3b), as in CeRhIn₅ at pressures above P_c , we associate $T_L(P)$ with $E_{\text{loc}}(P)$ in Sn-doped CeRhIn₅. In contrast to CeRhIn₅, $E_{\text{loc}}(P)$ extrapolates to $T = 0$ K at a distinctly lower pressure P_{c1} (~ 1.0 GPa) than the critical pressure P_{c2} where AFM transition is suppressed to $T = 0$ K. The termination of E_{loc} at P_{c1} indicates that a local-to-itinerant transformation of $4f$ degrees-of-freedom and concomitant reconstruction of FS take place within the AFM state of the Sn-doped material.

The existence of two critical pressures in Sn-doped CeRhIn₅ is supported by the low-temperature resistivity ρ_{ab} measured parallel to the Ce-In plane under a magnetic field of 4.9 T (Supplementary Fig. 6). The color contour of isothermal resistivity in the T - P plane, illustrated in Fig. 4a, shows a funnel of enhanced scattering centered at P_{c1} . The local temperature exponent n derived from $n = \partial(\ln\Delta\rho)/\partial(\ln T)$, in contrast, reveals a funnel of non-Fermi-liquid behavior centered near P_{c2} where the resistivity exhibits a linear-in- T dependence, illustrated in Fig. 4b. Figures 4d,g show ρ_{ab} as a function of temperature at representative pressures of 0.20, 1.38, 1.45, and 2.30 GPa, respectively. A Landau-Fermi-liquid T^2 dependence is observed at low- and high-pressure regimes in Figs. 4d,g, but the linear- T dependence is prominent near P_{c2} in Figs. 4e,f. Figure 4c summarizes the dependence on pressure of the residual resistivity ρ_0 on the left ordinate and the temperature coefficient A on the right ordinate estimated from a fit to $\rho_{\text{ab}} = \rho_0 + AT^n$. With increasing pressure, ρ_0 increases by over a factor of two, reaches a maximum at 1.0 GPa ($=P_{c1}$), and decreases with increasing pressure, reflecting enhanced scattering of critical charge fluctuations around P_{c1} ⁸⁻¹¹. The coefficient A , which is related to the effective mass of quasiparticles^{19,33}, however, gradually increases at low pressures, goes through a local minimum at P_{c1} , and peaks sharply at P_{c2} , which is consistent with the divergence of effective mass predicted at an SDW QCP.

Discussion

Despite several quantum-critical heavy-fermion candidates, the delocalization energy scale E_{loc} has been identified in a limited number of compounds, including YbRh₂Si₂^{13,14,18}, Ce₃Pd₂₀Si₆³⁴, and CeIn₃^{17,31}. In the case of YbRh₂Si₂, E_{loc} manifests as anomalies in isothermal measurements, such as a step-like crossover in the field-dependent Hall coefficient and magnetoresistivity that

sharpens with decreasing temperature or a smeared kink in the field-dependent Hall resistivity, magnetostriction, and magnetization^{13,14,18}. The locus of E_{loc} points extrapolates to a field-tuned zero-temperature boundary of magnetic order, as in CeRhIn₅ under applied pressure. Similar analysis of Hall data for Ce₃Pd₂₀Si₆ finds, however, that E_{loc} extrapolates inside the ordered part of its field-dependent phase diagram³⁴, analogous to Sn-doped CeRhIn₅ (Fig. 3c). This also is the case with pressure-tuned CeIn₃, discussed earlier, where a localization/delocalization scale intersects its antiferromagnetic phase at finite temperature^{17,31}.

In these other examples, the signature for E_{loc} in various physical quantities has been used to infer a Fermi-surface change, but dHvA measurements unambiguously establish a jump in dHvA frequencies at the critical pressure where T_L extrapolates to $T = 0$ K in CeRhIn₅. A simple interpretation of R_H would anticipate an associated step-like jump in carrier density at P_c , but as shown in Fig. 5a, instead of having a sharp jump, the pressure-dependent isothermal Hall coefficient peaks strongly at P_c . Perhaps measurements have not been made at sufficiently low temperatures to reveal a jump. More likely it is obscured by effects of critical charge and spin fluctuations on the Hall resistivity and/or only a small net change in the sum of hole and electron contributions in this nearly compensated metal. Though present experiments cannot make a definitive distinction, they do reflect the approach to FS reconstruction detected in dHvA that is coincident with a magnetic QCP. In contrast to the sharp peak in $|R_H(P)|$ in CeRhIn₅, there is a broad maximum $|R_H(P)|$ that peaks at P_{c1} but encompasses both P_{c1} and P_{c2} in CeRh(In_{0.956}Sn_{0.044})₅ (Fig. 5b). Such a broad maximum relative to that in CeRhIn₅ is not surprising because of the close proximity of two critical pressures, each with their own spectrum of critical spin/charge fluctuations, and smearing these spectra by disorder inherent to the Sn substitution.

The distinctly different critical behaviors of pure and Sn-doped CeRhIn₅ are captured in a generalized quantum-critical phase diagram that includes both Kondo-breakdown and SDW criticality^{8,35}. In this theory, the nature of quantum criticality is determined by two quantities, δ and G (Supplementary Fig. 9), where, as before, $\delta = k_B T_K / I$, and G is a parameter that reflects magnetic frustration or effective spatial dimensionality. Our results are consistent with Kondo breakdown coinciding in pure CeRhIn₅ under pressure with a $T = 0$ K transition from an AFM state with a small FS (AFM_S) to a paramagnetic state with a large FS (P_L) at P_c , i.e., Kondo

breakdown and the AFM QCP coincide. Similar to Sn-doped CeCoIn₅³⁶, Sn substitution for In in CeRhIn₅ enhances hybridization between 4*f*- and conduction electron wave functions, i.e., increases T_K and thus δ . Stronger hybridization also reduces frustration among magnetic exchange pathways^{8,37}. Analysis of magnetic neutron-diffraction experiments finds a clear change in magnetic structure and decrease of the ordered moment for a Sn concentration $x \geq 0.052$, comparable to CeRh(In_{0.956}Sn_{0.044})₅ under a modest pressure, that is attributed to an abrupt modification of the Fermi surface³⁸. With these changes induced by Sn doping, the system follows a different trajectory that goes through an intermediate magnetically ordered state with a large FS (AFM_L), i.e., Kondo breakdown occurs inside the AFM region, and thus the corresponding AFM QCP is of the SDW type as illustrated in Fig. 1a and Supplementary Fig. 9 and found in the prototypical Kondo-breakdown system YbRh₂Si₂ when Rh is replaced by a small amount of Co¹⁸.

Before identifying the crossover scale E_{loc} in pure and Sn-doped CeRhIn₅, their criticality was ambiguous, possibly either Kondo-breakdown or SDW^{32,39}. That ambiguity now is removed, with consequences for an interpretation of the origin of their pressure-induced superconductivity. At the SDW QCP in Sn-doped CeRhIn₅, which is decoupled from the Kondo breakdown and where T_c reaches its maximum, quantum fluctuations of the magnetic order parameter are the prime candidate for mediating Cooper pairing⁴⁰. Fluctuations around a Kondo-breakdown QCP, however, are far more complex and involve not only quantum-critical fluctuations of a magnetic order parameter but also of the Fermi surface, i.e., charge degrees-of-freedom⁸⁻¹¹. Initial model calculations show that critical Kondo-breakdown fluctuations can produce a superconducting instability^{41,42}, but much remains to make these calculations directly testable by experiment. Interestingly, $T_c \approx 2.3$ K of CeRhIn₅ at P_c and of CeCoIn₅ at $P = 0$ GPa is among the highest of any rare-earth-based heavy-fermion superconductor.

The theory of Kondo-breakdown criticality in heavy-fermion materials has two essential signatures – an abrupt change from small-to-large Fermi surface coincident with magnetic criticality and the charge delocalization crossover scale E_{loc} that extrapolates from the paramagnetic state to the QCP⁶. Without both, Kondo-breakdown criticality cannot be established with certainty. Our Hall measurements provide compelling evidence for E_{loc} in pure and Sn-doped CeRhIn₅ and, in light of dHvA results¹⁵, for Kondo-breakdown criticality in

CeRhIn₅. Finally, we speculate that critical charge fluctuations at a Kondo-breakdown QCP, evidenced by ω/T scaling of the frequency (ω)-dependent optical conductivity¹⁰, should play a non-trivial role in these signatures for E_{loc} . Making this connection experimentally and theoretically would mark a significant advance.

Methods

Single crystals of pure and Sn-doped CeRhIn₅ were synthesized using the standard self-flux technique³². The high-pressure resistivity and Hall measurements on CeRhIn₅ were carried out using the Van der Pauw method⁴³ in a diamond-anvil cell made of Be-Cu alloy. NaCl powder was applied as the pressure medium to obtain a quasihydrostatic pressure environment. The pressure in the diamond-anvil cell was determined by the ruby fluorescence method⁴⁴. The high-pressure resistivity and Hall measurements on CeRh(In_{0.956}Sn_{0.044})₅ were measured using the standard six-probe method in a Be-Cu/NiCrAl hybrid clamp-type cell. Daphne oil was employed as the pressure medium to obtain a hydrostatic pressure environment. The pressure dependence of the superconducting transition temperature of Pb was used to determine the pressure inside the clamp-type cell⁴⁵. All measurements were performed with a low-frequency resistance bridge from Lake Shore Cryotronics. A ⁴He cryostat without magnetic field and a Physical Property Measurement System with a maximum magnetic field of 9 T were used in the temperature range of 1.8 to 300 K. A HelioxVL system with a maximum magnetic field of 12 T was used to control temperature down to 0.3 K.

Data availability

All data supporting the findings of this study are available within the article and the supplementary information. The data are available upon request to the corresponding authors.

Acknowledgements

This work was supported by Basic Science Research Program through the National Research Foundation of Korea (NRF) funded by the Ministry of Education (No. 2021R111A1A01047499 (H.W.)) and by the National Research Foundation of Korea (NRF) grant funded by the Korea government (MSIT) (No. 2021R1A2C2010925 (T.P.) and No. RS-2023-00220471 (T.P.)).

Work at Los Alamos was performed under the auspices of the U.S. Department of Energy, Office of Basic Energy Sciences, Division of Materials Science and Engineering.

Author contributions

All authors discussed the results and commented on the manuscript. T.P. and H.W. conceived the study. T.B.P. and H.W. performed the measurements and analyzed the data. J.K. and H.J. assisted the transport measurements setup. T.B.P. and E.D.B. synthesized pure and Sn-doped CeRhIn₅ single crystals. H.W., T.B.P., T.P., and J.D.T. wrote the manuscript with input from all authors.

Competing interests: The authors declare no competing interests.

References

1. Affleck, I. The Kondo screening cloud: what it is and how to observe it. In *Perspectives of Mesoscopic Physics* (eds Aharony, A. & Entin-Wohlman, O.) Ch. 1, 1-44 (World Scientific, 2010).
2. Borzenets, I. V. et al. Observation of the Kondo screening cloud. *Nature* **579**, 210-213 (2020).
3. Millis, A. J. Effect of a nonzero temperature on quantum critical points in itinerant fermion systems. *Phys. Rev. B* **48**, 7183 (1993).
4. Coleman, P., Pépin, C., Si, Q. & Ramazashvili, R. How do Fermi liquids get heavy and die? *J. Phys.: Condens. Matter* **13**, R723-R738 (2001).
5. Löhneysen, H. v., Rosch, A., Vojta, M. & Wölfle, P. Fermi-liquid instabilities at magnetic quantum phase transitions. *Rev. Mod. Phys.* **79**, 1015 (2007).
6. Si, Q., Rabello, S., Ingersent, K. & Smith, J. L. Locally critical quantum phase transitions in strongly correlated metals. *Nature* **413**, 804-808 (2001).
7. Gegenwart, P., Si, Q. & Steglich, F. Quantum criticality in heavy-fermion metals. *Nat. Phys.* **4**, 186-197 (2008).
8. Coleman, P. & Nevidomskyy, A. H. Frustration and the Kondo effect in heavy fermion materials. *J. Low Temp. Phys.* **161**, 182-202 (2010).
9. Komijani, Y. & Coleman, P. Emergent critical charge fluctuations at the Kondo breakdown of heavy fermions. *Phys. Rev. Lett.* **122**, 217001 (2019).
10. Prochaska, L. et al. Singular charge fluctuations at a magnetic quantum critical point. *Science* **367**, 285-288 (2020).
11. Paschen, S. & Si, Q. Quantum phases driven by strong correlations. *Nat. Rev. Phys.* **3**, 9-26 (2021).
12. Schröder, A. et al. Onset of antiferromagnetism in heavy-fermion metals. *Nature* **407**, 351-355 (2000).
13. Paschen, S. et al. Hall-effect evolution across a heavy-fermion quantum critical point. *Nature* **432**, 881-885 (2004).
14. Gegenwart, P. et al. Multiple energy scales at a quantum critical point. *Science* **315**, 969-971 (2007).

15. Shishido, H., Settai, R., Harima, H. & Ōnuki, Y. A drastic change of the Fermi surface at a critical pressure in CeRhIn₅: dHvA study under pressure. *J. Phys. Soc. Jpn.* **74**, 1103-1106 (2005).
16. Park, T. et al. Isotropic quantum scattering and unconventional superconductivity. *Nature* **456**, 366-368 (2008).
17. Kawasaki, S. et al. Pressure-induced unconventional superconductivity in the heavy-fermion antiferromagnet CeIn₃: An ¹¹⁵In-NQR study under pressure. *Phys. Rev. B* **77**, 064508 (2008).
18. Friedemann, S. et al. Detaching the antiferromagnetic quantum critical point from the Fermi-surface reconstruction in YbRh₂Si₂. *Nat. Phys.* **5**, 465-469 (2009).
19. Luo, Y. et al. Unconventional and conventional quantum criticalities in CeRh_{0.58}Ir_{0.42}In₅. *npj Quantum Mater.* **3**, 6 (2018).
20. Kawasaki, S. et al. Localized-to-itinerant transition preceding antiferromagnetic quantum critical point and gapless superconductivity in CeRh_{0.5}Ir_{0.5}In₅. *Commun. Phys.* **3**, 148 (2020).
21. Park, T. et al. Hidden magnetism and quantum criticality in the heavy fermion superconductor CeRhIn₅. *Nature* **440**, 65-68 (2006).
22. Knebel, G., Aoki, D., Braithwaite, D., Salce, B. & Flouquet, J. Coexistence of antiferromagnetism and superconductivity in CeRhIn₅ under high pressure and magnetic field. *Phys. Rev. B* **74**, 020501(R) (2006).
23. Watanabe, H. & Ogata, M. Fermi-surface reconstruction without breakdown of Kondo screening at the quantum critical point. *Phys. Rev. Lett.* **99**, 136401 (2007).
24. Nakajima, Y. et al. Non-Fermi liquid behavior in the magnetotransport of CeMIn₅ (M: Co and Rh): striking similarity between quasi two-dimensional heavy fermion and high-*T_c* cuprates. *J. Phys. Soc. Jpn.* **76**, 024703 (2007).
25. Bao, W. et al. Anisotropic three-dimensional magnetic fluctuations in heavy fermion CeRhIn₅. *Phys. Rev. B* **65**, 100505(R) (2002).
26. Kawasaki, S. et al. The phase diagram of antiferromagnetism and superconductivity in CeRhIn₅: a study of ¹¹⁵In NQR under pressure. *J. Phys.: Condens. Matter* **17**, S889 (2005).
27. Hundley, M. F., Malinowski, A., Pagliuso, P. G., Sarrao, J. L. & Thompson, J. D. Anomalous *f*-electron Hall effect in the heavy-fermion system CeTIn₅ (T=Co, Ir, or Rh). *Phys. Rev. B* **70**, 035113 (2004).

28. Park, T. et al. Unconventional quantum criticality in the pressure-induced heavy-fermion superconductor CeRhIn₅. *J. Phys.: Condens. Matter* **23**, 094218 (2011).
29. Pham, L. D., Park, T., Maquilon, S., Thompson, J. D. & Fisk, Z. Reversible tuning of the heavy-fermion ground state in CeCoIn₅. *Phys. Rev. Lett.* **97**, 056404 (2006).
30. Maksimovic, N. et al. Evidence for a delocalization quantum phase transition without symmetry breaking in CeCoIn₅. *Science* **375**, 76-81 (2022).
31. Araki, S., Onji, T., Kitagawa, S., Kobayashi, T. C. & Kambe, T. Hall effect in CeIn₃ under high pressure. *J. Phys. Soc. Jpn.* **84**, 123702 (2015).
32. Bauer, E. D. et al. Antiferromagnetic quantum critical point in CeRhIn_{5-x}Sn_x. *Phys. B: Condens. Matter* **378-380**, 142-143 (2006).
33. Grigera, S. A. et al. Magnetic field-tuned quantum criticality in the metallic ruthenate Sr₃Ru₂O₇. *Science* **294**, 329-332 (2001).
34. Custers, J. et al. Destruction of the Kondo effect in the cubic heavy-fermion compound Ce₃Pd₂₀Si₆. *Nat. Mater.* **11**, 189-194 (2012).
35. Si, Q. Quantum criticality and global phase diagram of magnetic heavy fermions. *Phys. Status Solidi B* **247**, 476-484 (2010).
36. Chen, K. et al. Evolution of ground-state wave function in CeCoIn₅ upon Cd or Sn doping. *Phys. Rev. B* **97**, 045134 (2018).
37. Das, P. et al. Magnitude of the magnetic exchange interaction in the heavy-fermion antiferromagnet CeRhIn₅. *Phys. Rev. Lett.* **113**, 246403 (2014).
38. Raymond, S. et al. Switching of the magnetic order in CeRhIn_{5-x}Sn_x in the vicinity of its quantum critical point. *Phys. Rev. B* **90**, 014423 (2014).
39. Seo, S. et al. Controlling superconductivity by tunable quantum critical points. *Nat. Commun.* **6**, 6433 (2015).
40. Monthoux, P., Pines, D. & Lonzarich, G. G. Superconductivity without phonons. *Nature* **450**, 1177-1183 (2007).
41. Pixley, J. H., Deng, L., Ingersent, K. & Si, Q. Pairing correlations near a Kondo-destruction quantum critical point. *Phys. Rev. B* **91**, 201109(R) (2015).
42. Hu, H. et al. Unconventional superconductivity from Fermi surface fluctuations in strongly correlated metals. Preprint at <https://10.48550/arXiv.2109.13224> (2021).
43. van der Pauw, L. J. A method of measuring the resistivity and Hall coefficient on lamellae of arbitrary shape. *Philips Tech. Rev.* **20**, 220-224 (1958).

44. Mao, H. K., Xu, J. & Bell, P. M. Calibration of the ruby pressure gauge to 800 kbar under quasi-hydrostatic conditions. *J. Geophys. Res. Solid Earth* **91**, 4673-4676 (1986).
45. Eiling, A. & Schilling, J. S. Pressure and temperature dependence of electrical resistivity of Pb and Sn from 1-300K and 0-10 GPa-use as continuous resistive pressure monitor accurate over wide temperature range; superconductivity under pressure in Pb, Sn and In. *J. Phys. F. Met. Phys.* **11**, 623-639 (1981).

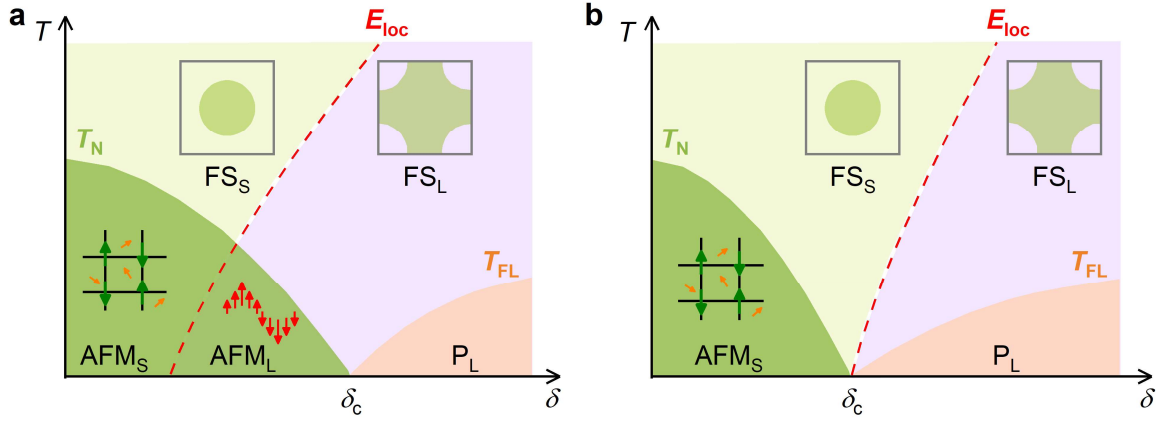


Fig. 1 Schematic phase diagrams of two classes of QCPs in AFM heavy-fermion metals.

Under the variation of the non-thermal parameter δ , an AFM transition is continuously suppressed to zero temperature at a critical value δ_c . Consequently, an AFM QCP appears at δ_c and the ground state changes from an AFM to a paramagnetic Fermi-liquid (FL) state. T_N and T_{FL} represent the AFM transition temperature and the onset temperature of the FL regime, respectively. E_{loc} denotes the Kondo destruction energy scale that is associated with delocalization of the local moment. In a sufficiently low-temperature regime, $E_{loc}(\delta)$ separates the Kondo-screened regime with a large FS (FS_L , $4f$ -electrons delocalized, right side of the $E_{loc}(\delta)$ line) and the Kondo-destruction regime with a small FS (FS_S , $4f$ -electrons localized, left side of the $E_{loc}(\delta)$ line). The ground state is divided into three phases: an AFM phase with a small FS (AFM_S), an AFM phase with a large FS (AFM_L), and a paramagnetic phase with a large FS (P_L). **a**, For the conventional SDW type QCP, $E_{loc}(\delta)$ terminates inside the AFM regime. **b**, For a Kondo-breakdown type QCP, $E_{loc}(\delta)$ terminates at the AFM QCP. Top and bottom insets show cartoon pictures of the FS and the spin fluctuations in the different phases. Olive, orange, and red arrows indicate the local moments, the itinerant conduction electrons, and the magnetic moments screened by the conduction electrons, respectively.

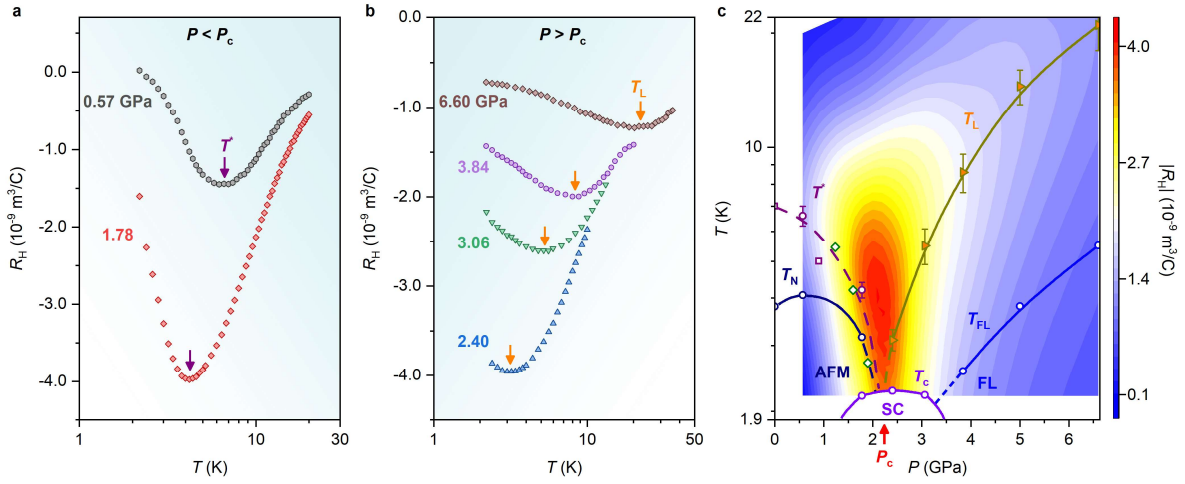


Fig. 2 Evolution of the Hall coefficient with pressure and the T - P phase diagram for CeRhIn₅. **a,b**, Temperature dependence of Hall coefficient R_H for CeRhIn₅ at representative pressures measured at temperatures above the superconducting transition temperature T_c and under a magnetic field of 1 T applied along the c -axis. The field is much lower than those required to observe quantum oscillations¹⁵ and to suppress superconductivity²¹. The purple and orange arrows represent the onset of short-range AFM spin correlations at T^* and the $4f$ -electron delocalization crossover temperature T_L , respectively (see text for details). **c**, T - P phase diagram of CeRhIn₅ at 0 T overlaid with a contour plot of the amplitude of the Hall coefficient $|R_H|$ at 1 T. T^* , T_N , T_L , T_c , and T_{FL} are denoted by purple circles, navy circles, orange triangles, violet circles, and blue circles, respectively. Kondo breakdown and the AFM QCP coincide at the critical pressure P_c where T_c reaches a maximum, the Fermi surface reconstructs from small-to-large, and temperature T_L of the local extremum in $|R_H|$ extrapolates to zero temperature. The purple squares and olive diamonds are data adopted from Hall²⁴ and nuclear quadrupole resonance²⁶ measurements, respectively. The dashed and solid lines are guides to the eyes. AFM, SC, and FL stand for antiferromagnetic, superconducting, and Fermi liquid regions, respectively. Error bars on the T^* and T_L represent the uncertainties in determining the minimum in the Hall coefficient.

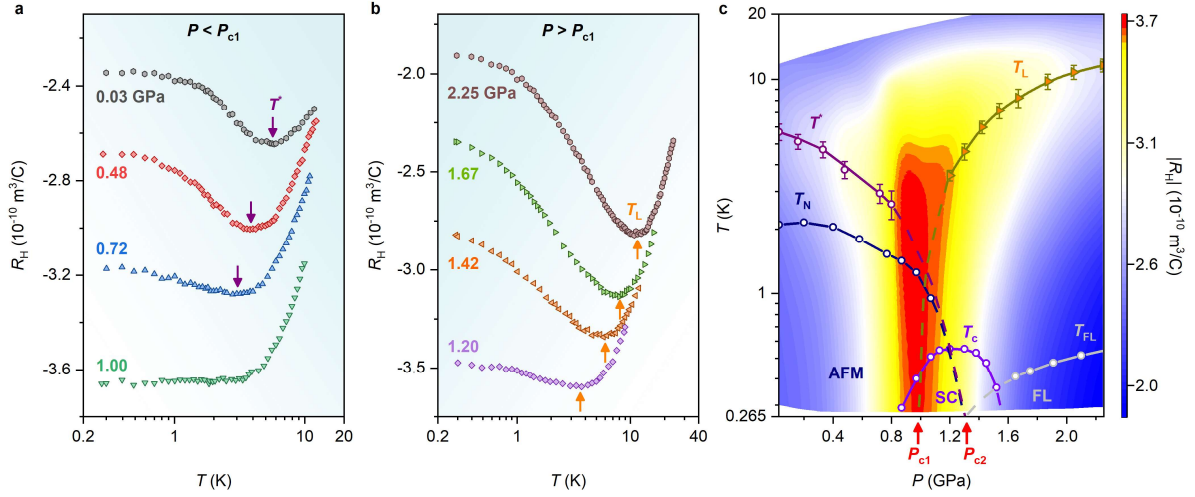


Fig. 3 Evolution of the Hall coefficient with pressure and the T - P phase diagram for Sn-doped CeRhIn₅. **a,b**, Hall coefficient R_H of Sn-doped CeRhIn₅ measured at 5 T is plotted as a function of temperature at representative pressures. The purple and orange arrows represent the onset of short-range magnetic correlations at T^* and the $4f$ -electron delocalization crossover temperature T_L , respectively (see text for details). **c**, T - P phase diagram of Sn-doped CeRhIn₅ at 0 T overlaid with a contour plot of the amplitude of the Hall coefficient $|R_H|$ at 5 T. T^* , T_N , T_L , T_c , and T_{FL} are denoted by purple circles, navy circles, orange triangles, violet circles, and gray circles, respectively. P_{c2} (~ 1.3 GPa) is the critical pressure where T_N extrapolates to zero temperature, corresponding to an SDW QCP, and T_c reaches a maximum. P_{c1} (~ 1.0 GPa) is another critical pressure where $T_L(P)$ extrapolates to zero temperature, indicating that destruction of the Kondo effect occurs within the AFM phase. The dashed and solid lines are guides to the eyes. AFM, SC, and FL stand for antiferromagnetic, superconducting, and Fermi liquid regions, respectively. Error bars on the T^* and T_L represent the uncertainties in determining the minimum in the Hall coefficient.

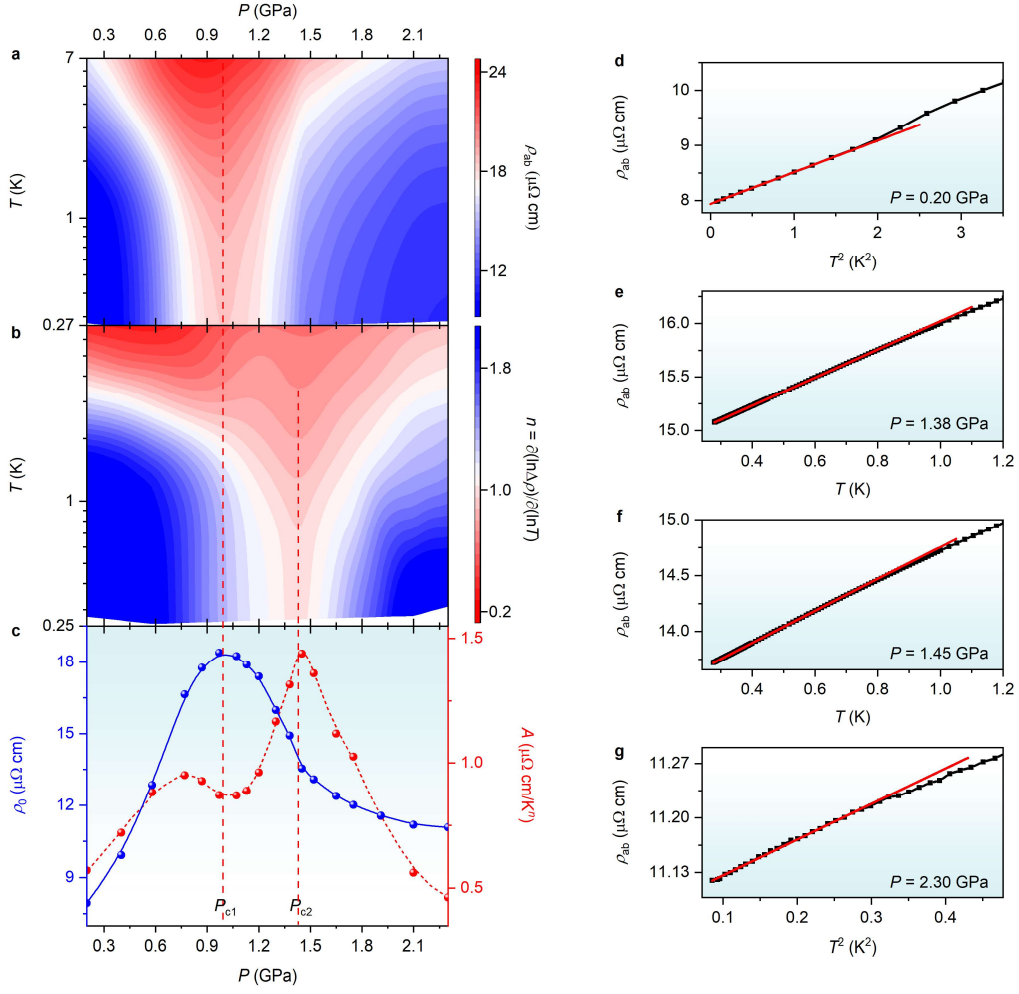


Fig. 4 Quantum criticality of Sn-doped CeRhIn₅ under pressure. **a**, Contour plot of resistivity ρ_{ab} for Sn-doped CeRhIn₅ measured parallel to the Ce-In plane under a magnetic field of 4.9 T. The significant enhancement of ρ_{ab} is centered around P_{c1} . **b**, Colours represent the local temperature exponent n derived from $n = \partial(\ln\Delta\rho)/\partial(\ln T)$, where $\Delta\rho = \rho_{ab} - \rho_0 = AT^n$ and ρ_0 is the residual resistivity. A funnel regime with linear- T dependence of ρ_{ab} is observed around P_{c2} , a characteristic of the non-Fermi liquid behavior near the AFM QCP, as shown in **(e)** and **(f)** at representative pressures of 1.38 and 1.45 GPa, respectively. **c**, Pressure dependence of the residual resistivity ρ_0 (left-axis, blue circles) and the coefficient A (right-axis, red circles) determined by fitting the low-temperature resistivity to $\rho_{ab} = \rho_0 + AT^n$. **d–g** show fits to representative data from which **(c)** is constructed. The dashed red lines in **(a–c)** are guides to the eyes. The red lines in **(d–g)** are least-squares fits to the low-temperature data.

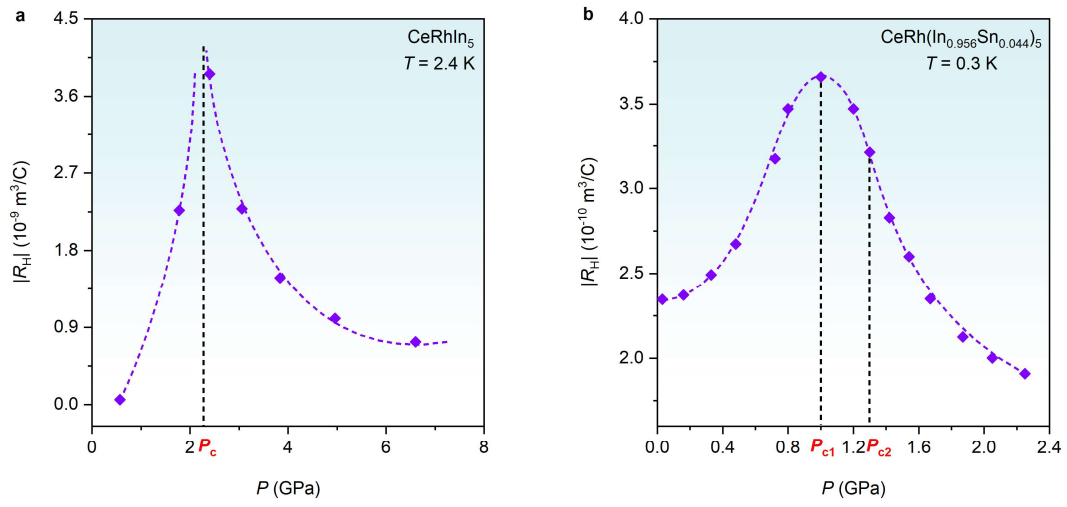


Fig. 5 Isothermal pressure dependence of the Hall coefficient. a, Pressure dependence of Hall coefficient $|R_H(P)|$ for CeRhIn_5 at 2.4 K. P_c indicates the magnetic QCP. **b,** Pressure dependence of Hall coefficient $|R_H(P)|$ for $\text{CeRh}(\text{In}_{0.956}\text{Sn}_{0.044})_5$ at 0.3 K. P_{c2} denotes the magnetic QCP. P_{c1} indicates the critical pressure where T_L extrapolates to zero temperature and is lower than the magnetic QCP P_{c2} .